Restoration of Images with Piecewise Space-Variant Blur

Leah Bar[1], Nir Sochen[2], and Nahum Kiryati[3]

[1] Department of Electrical and Computer Engineering,
University of Minnesota, Minneapolis, MN 55455, USA
[2] Dept. of Applied Mathematics
[3] School of Electrical Engineering
Tel Aviv University, Tel Aviv 69978, Israel

Abstract. We address the problem of space-variant image deblurring, where different parts of the image are blurred by different blur kernels. Assuming a region-wise space variant point spread function, we first solve the problem for the case of known blur kernels and known boundaries between the different blur regions in the image. We then generalize the method to the challenging case of unknown boundaries between the blur domains. Using variational and level set techniques, the image is processed globally. The space-variant deconvolution process is stabilized by a unified common regularizer, thus preserving discontinuities between the differently restored image regions. In the case where the blurred subregions are unknown, a segmentation procedure is performed using an evolving level set function, guided by edges and image derivatives.

1 Introduction

Most image deblurring methods rely on the standard model of a space invariant kernel and additive noise

$$g = h * f + n. \tag{1}$$

Here h denotes a known space-invariant blur kernel, f is an ideal version of the observed image g, and n is noise. Yet, the assumption of space-invariance is not accurate in real photographic images. For example, when multiple objects move at different velocities and in different directions in a scene, one gets space-variant motion blur. Likewise, when a camera lens is focused on one specific object, other objects nearer or farther away from the lens are not as sharp. In such situations, different blur kernels degrade different areas of the image. Other applications include astronomy [12] and medical (SPECT) imaging [21]. In the space-variant case, assuming a linear blur, Eq. (1) takes the form

$$g(x) = \int h(x, x-u) f(u) du + n,$$

where x is a location in the observed image and u is a location in the ideal image f.

Most of the space-variant deconvolution literature considers the space-variant problem under the assumption that the blur function is known. For example, Nagy and O'leary developed a fast deconvolution algorithm via matrix-vector multiplication involving banded Toeplitz matrices [14]. The blurring kernels are assumed to have small domain of support. Lauer [12] dealt with astronomical images and modeled the point spread function (PSF) as a sum of orthogonal functions. Welk *et al.* [20] presented a variational deblurring method such that the recovered image f was the minimizer of an objective functional that consists of a robust fidelity term and a Perona-Malik regularizer [16].

Few works address the blind space-variant deconvolution issue. You and Kaveh [22] presented a variational approach to this problem. In their method, a parametric space-variant PSF with piecewise smooth space variance constraint is utilized. In the case of motion blur, for example, the velocity $v(x)$ was calculated. This approach, however, suffers from severe multiple local minima problems.

Favaro and Soatto [7] presented a variational approach to segmentation and restoration of scenes containing multiple moving objects. From a collection of motion blurred images, they calculate the motion field, depth map and radiance. In their method, the blur kernel is *implicitly* formulated in the objective functional. The idea of simultaneous variational restoration and segmentation was first introduced by Kim *et al.* [10]; they used a variant of the Mumford-Shah functional [13] together with a curve evolution technique, but assumed a *known space-invariant* blur kernel.

A significant contribution to the related *shape from defocus* problem was given by Favaro *et al.* The 3D shape of a scene was estimated from a collection of defocused images [8, 9]. In the case of a moving scene, the depth map, radiance and motion was inferred via an anisotropic diffusion model from a collection of defocused and motion-blurred images [4].

Schechner *et al.* [18] presented an algorithm for the separation of two transparent layers. Nonetheless, their work assumes that two images are available such that in each image one layer is in focus.

Here we propose a novel variational approach to space-variant restoration. The underlying model of this work assumes a space-variant PSF with piecewise location dependence. This means that every sub-domain in the image is blurred by a different kernel. The regions are separated by contours that are expressed as zero level set functions. First we will solve the case where the contours and blur kernels are known in advance. The contribution of the proposed non-blind space-variant restoration approach relies on the usage of a global regularizer, which eliminates the requirement of dealing with region boundaries. As a result, the gray levels continuity of the recovered image is inherent. This method does not limit the number of sub-regions, their geometrical shape nor the kernel support size. In addition, since the restoration is global, the convolution operation can be efficiently implemented by using Fast Fourier Transform (FFT) multiplications.

In the second part of the paper, we will address the blur segmentation given a *single* image. We assume two sub-regions and known or easily estimated blur kernels but an unknown contour between the sub-regions. The blur level differ-

ence between the regions is assumed to be visually significant. This problem is approached via a sequential process. We first segment the observed image into its blurred sub-regions. The boundaries are determined using an evolving level set function, guided by edges and image derivatives. Then we use the suggested non-blind space-variant restoration method given the sub-regions and estimated blur kernels. The advantage of this approach over a one-step process is the additional regularization of this ill-posed problem. In the contours detection stage, some assumptions are made regarding the contour properties. Pre-detected edges and derivatives provide additional important information on this process. In such a manner, the solutions space is reduced. The suggested method accommodates arbitrary blur functions. It is because the contour detection process depends essentially on the blur level rather on the blur type.

2 Non-Blind Space-Variant Restoration

Consider an image that consists of known sub-domains blurred by known kernels. It is well known [14] that region-wise deblurring may yield boundary discontinuities. This problem is illustrated in Fig. 1. The 256×256 *Lena* image was blurred by an 8 pixels horizontal motion blur within the marked rectangular region. This region was recovered by the Total Variation deconvolution method [19] and put back into its place in the observed image. The outcome of the region-wise procedure is shown on the right. It can be easily seen that although the regional recovery is satisfying, the gray levels on both sides of the boundary are not compatible. To solve this problem, some blending constraints have to be added to the boundary conditions. Moreover, if the region shape is more complex, dealing with boundaries requires additional algorithmic effort.

Fig. 1. Failure of the region-wise image deconvolution algorithm. *Left:* Spatially variant blurred image. *Right*: Restoration using a region-wise algorithm

In the current study, we suggest a variational setting in which a global regularizer automatically takes care of gray level continuity in region boundaries.

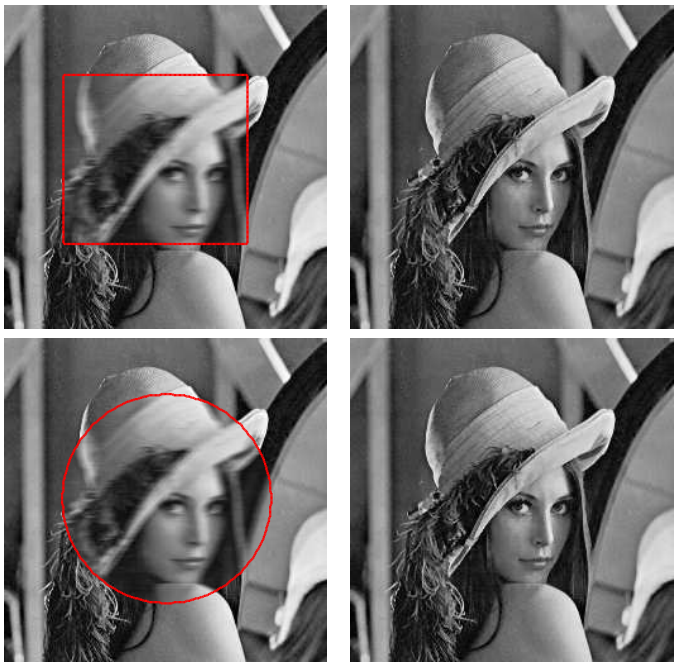

Fig. 2. Non-blind space-variant restoration. *Left column*: Spatially variant motion blurred images. *Right column:* The corresponding recovered images using the suggested method.

Furthermore, there are no limitations on the number and shapes of the blur regions.

Let us define Ω as an open bounded set in $\mathbb{R}^n$, and an image $f(x) : \Omega \to \mathbb{R}^n$. The open non-overlapping subsets $w_i \subset \Omega$ denote regions that are blurred by kernels h_i respectively. In addition, $\Omega \setminus \cup\overline{w_i}$, denotes the background region blurred by the background kernel h_b, and $\overline{w_i}$ stands for the closure of w_i. The region boundaries are designated by ∂w_i. Deconvolution is known to be an ill-posed inverse problem that has to be regularized. In the variational framework, the recovered image is the minimizer of an objective functional that consists of a fidelity term $\mathcal{T}$ and a regularizer $\mathcal{R}$ that reflects some *a priori* knowledge about the image, such as smoothness. Boundary discontinuities can be prevented by using a global regularizer. This means that the smoothness constraint is applied to the whole image. Formally, the fidelity term is given by

$$\mathcal{T} = \frac{1}{2}\sum_i \eta_i \int_{w_i} (h_i * f - g)^2 dx + \frac{\eta_b}{2} \int_{\Omega\setminus(\cup\overline{w_i})} (h_b * f - g)^2 dx, \qquad (2)$$

where η_i and η_b are positive scalars.

Using the level set framework [15], the region boundaries ∂w_i can be implicitly represented by Lipschitz functions $\phi_i : \Omega \to \mathbb{R}$, such that

$$C_i \doteq \partial w_i = \{x \in \Omega : \phi_i(x) = 0\}.$$

Following the formulation of Chan and Vese [6], the domains w_i can be replaced by the Heaviside function $H(\phi_i)$, where

$$H(\phi_i) = \begin{cases} 1, & \phi_i > 0, \\ 0, & \phi_i \leq 0. \end{cases} \tag{3}$$

The fidelity term $\mathcal{T}$ can, therefore, be rewritten as

$$\begin{aligned} \mathcal{T} = & \frac{1}{2} \sum_i \eta_i \int_\Omega (h_i * f - g)^2 H(\phi_i) dx \\ & + \frac{\eta_b}{2} \int_\Omega (h_b * f - g)^2 \left(1 - \sum_i H(\phi_i)\right) dx. \end{aligned} \tag{4}$$

Several edge preserving regularizers are known to be effective in image restoration and denoising. The Total Variation [17] and Perona-Malik [16] stabilizers, for example, are widely used in the scientific literature. Here we favor the recently proposed Mumford-Shah [13] based regularizer that is used for the deblurring process [2]. In this approach, the image is modeled as a piecewise smooth function, that is the observed image can be decomposed into smooth regions by well-behaved contours. The regularizer is expressed as

$$\mathcal{R}^{MS} = \beta \int_{\Omega \setminus K} |\nabla f|^2 dx + \alpha \int_K d\sigma$$

where K denotes the unknown edge set and $\int_K d\sigma$ is the total edge length. The Mumford-Shah regularizer, which leads to a free discontinuity problem, can be approximated by a regular functional in the Γ-convergence framework [3]. Ambrosio and Tortorelli [1] approximated the irregular regularizer by a sequence $\mathcal{R}_\epsilon$ where $\epsilon \to 0$. The edge set K is represented by the characteristic function $(1 - \chi_K)$, which in turn is approximated by a smooth auxiliary function v such that $v \approx 0$ across the edges and $v \approx 1$ within the segments. The approximated regularizer thus takes the form

$$\mathcal{R}_\epsilon^{MS} = \beta \int_\Omega v^2 |\nabla f|^2 dx + \alpha \int_\Omega \left(\epsilon |\nabla v|^2 + \frac{(v-1)^2}{4\epsilon}\right) dx. \tag{5}$$

Hence, the objective functional $\mathcal{F}_\epsilon^{MS} \doteq \mathcal{T} + \mathcal{R}_\epsilon^{MS}$ is given by

$$\begin{aligned} \mathcal{F}_\epsilon^{MS}(f, v) = & \frac{1}{2} \sum_i \eta_i \int_\Omega (h_i * f - g)^2 H(\phi_i) dx \\ & + \frac{\eta_b}{2} \int_\Omega (h_b * f - g)^2 \left(1 - \sum_i H(\phi_i)\right) dx \\ & + \beta \int_\Omega v^2 |\nabla f|^2 dx + \alpha \int_\Omega \left(\epsilon |\nabla v|^2 + \frac{(v-1)^2}{4\epsilon}\right) dx. \end{aligned} \tag{6}$$

Whenever the contours C_i are known *a priori*, the ϕ_i functions can easily be determined. The recovered image f and edge map v are alternately obtained via the solution of the following Euler-Lagrange equations [2]:

$$\frac{\delta \mathcal{F}_\epsilon^{MS}}{\delta f} = \sum_i \eta_i h_i(-x) * [(h_i * f - g)H(\phi_i)] \tag{7}$$
$$+ \eta_b h_b(-x) * \left[(h_b * f - g) \left(1 - \sum_i H(\phi_i) \right) \right] - 2\beta \nabla \cdot (v^2 \nabla f) = 0,$$

$$\frac{\delta \mathcal{F}_\epsilon^{MS}}{\delta v} = 2\beta v |\nabla f|^2 + \alpha \cdot \frac{v-1}{2\epsilon} - 2\epsilon\, \alpha\, \nabla^2 v = 0. \tag{8}$$

Fig. 3. Non-blind space-variant restoration with different blur kernels in each region. *Left:* Blurred image. *Right:* Restoration using the suggested method.

Fig. 2 demonstrates the performance of the suggested algorithm. The two images in the left column were synthetically blurred by an 8 pixels length horizontal motion blur within the marked rectangle (top) and circle (bottom). The corresponding recovered images are shown in the right column. Since there was no background blur, h_b was as a delta function. The parameter set used was: $\eta_{1,b} = 1$, $\beta = 10^{-3}$, $\alpha = 10^{-8}$ and $\epsilon = 10^{-3}$. The superiority of this method over the region-wise approach (Fig. 1) is evident.

Fig. 3 demonstrates a more complex case. The ellipse and curve sub-regions were blurred by pill boxes of radius 4.9 and 2.1 pixels, respectively. The background blur was again a delta function. The image was recovered again with $\eta_{1,2,b} = 1$ and the same parameters set as before.

3 Blur Segmentation and Space-Variant Restoration

In this section, we address the problem of deblurring an image consisting of two *unknown* sub-regions blurred by different kernels. We assume that the blur level

Fig. 4. *Left:* Blurred image. *Right:* The corresponding E function.

difference between the regions is significant, and that both PSFs are known or can be easily estimated. We present a novel approach to detect the boundary between the sub-regions by the evolution of a level set function.

The key idea is to distinguish between different blur levels in the observed image. It is readily apparent that highly blurred regions accommodate low spatial derivatives. Edge information provides additional useful knowledge for the discrimination process. Let us define a function E such that

$$E \doteq \left|\log\left(\left|\nabla^2 g\right| * B_r\right)\right|, \tag{9}$$

and B_r is a ball of radius r. This function represents a smoothed version of the Laplacian of the observed image g. Fig. 4 illustrates E with $r = 2$ pixels. The two sub-regions are visibly distinguishable by their different gray levels. A closer look at E shows that the gray levels of the edges in both regions are darker than the segments, but the average value of the edges in the blurred sub-region is lighter than in the sharp sub-region. This observation motivated us to perform the contour detection by the difference of gray levels of E.

Let C denote the separating contour, K the edge set of the observed image, and $\overrightarrow{c} \doteq \{c_1, c_2, c_3, c_4\}$ the average gray levels of the edges inside the contour, the edges outside the contour, the segments inside the contour and the segments outside the contour respectively. Ideally, the separating contour C is the minimizer of the functional:

$$\begin{aligned}\mathcal{F}(C, \overrightarrow{c}) = {} & \frac{\lambda_1}{2}\int_{\text{inside}(C)\cap K}(E-c_1)^2 dx + \frac{\lambda_2}{2}\int_{\text{outside}(C)\cap K}(E-c_2)^2 dx \\ & + \frac{\lambda_3}{2}\int_{\text{inside}(C)\setminus K}(E-c_3)^2 dx + \frac{\lambda_4}{2}\int_{\text{outside}(C)\setminus K}(E-c_4)^2 dx \\ & - \underbrace{\oint_C |\langle \nabla E, \overrightarrow{n}\rangle| ds}_{\text{Robust Alignment}} + \underbrace{\oint \mathcal{G}(C(s) ds}_{\text{Geodesic Active Contour}} .\end{aligned} \tag{10}$$

The first four terms are fidelity terms that reflect the different gray levels in E. The fifth term is a robust alignment [11]. It integrates the absolute value of the inner product between the gradient of E and the curve normal $\overrightarrow{n}$ along the contour. This measure reflects the projection of the E gradients on the curve normals. Minimizing the minus of this term aligns these two vectors together.

The last term is the geodesic active contour [5], which is an integration of an *inverse* edge indicator function along the contour. A curve C that minimizes this term is the curve along which the edge indicator function is a local maximum. Fig. 4 shows that there is a significant gray level difference between the blurred sub-regions, which in is this case can be seen to be a circle. Thus, the geodesic active contour function must have low values along the separating contours. In its classical form, the geodesic function has low values along the image gradients, but in our case, the contribution from the edges needs to be eliminated. As a result, the active contour will eventually follow the separating contour. This is accomplished by detecting the edges in advance. We use the Mumford-Shah based non-blind space-invariant restoration method [2]. As noted before, in this framework edges are represented by a smooth function $v(x)$ where $v \approx 0$ across the edges and $v \approx 1$ within the segments. In an iterative process, both f and v are alternately calculated as the minimizers of the following objective functional

$$\begin{aligned}\mathcal{F}(f,v) = \frac{1}{2}\int_{\Omega}(g * B_r - h_b * f)^2 + \beta\int_{\Omega} v^2|\nabla f|^2 dx \\ + \alpha\int_{\Omega}\left(\epsilon|\nabla v|^2 + \frac{(v-1)^2}{4\epsilon}\right)dx.\end{aligned} \tag{11}$$

The g function was smoothed a little in order to get thicker edges. The blur kernel was selected to be the weaker of the two kernels (the background kernel in our example) to avoid over-deconvolution artifacts. Detailed minimization techniques can be found in [2]. Now, let

$$v_T = \begin{cases} 1, & v > T, \\ 0, & v \leq T, \end{cases} \tag{12}$$

be a binary edge map, where $v_T = 1$ in the segments and $v_T = 0$ across the edges.

We proceed to introducing the $\mathcal{G}$ function (for Eq. 10):

$$\mathcal{G}(\nabla E, v_T) = \frac{\mu}{1 + (v_T^2|\nabla E|^2)/\gamma} + \nu. \tag{13}$$

The constants γ, μ, ν are positive scalars. This inverse edge indicator function has low values along the separating contour because edge contributions are now eliminated by v_T.

As already noted, a contour C can be implicitly represented as the zero level set function $C = \{x \in \Omega : \phi(x) = 0\}$. In terms of a level set function [6]

$$\text{Length}\{C\} = \oint_C ds = \int_{\Omega}|\nabla H(\phi(x))|dx = \int_{\Omega}\delta(\phi(x))|\nabla\phi(x)|dx,$$

and the curve normal $\overrightarrow{n} = \nabla\phi/|\nabla\phi|$ [11]. Therefore, Eq. (10) can be rewritten as

$$\begin{aligned}\mathcal{F}(\phi, \overrightarrow{c}) = {} & \frac{\lambda_1}{2}\int_\Omega (1-v)^2(E-c_1)^2 H(\phi)dx + \frac{\lambda_2}{2}\int_\Omega (1-v)^2(E-c_2)^2(1-H(\phi))dx \\ & + \frac{\lambda_3}{2}\int_\Omega v^2(E-c_3)^2 H(\phi)dx + \frac{\lambda_4}{2}\int_\Omega v^2(E-c_4)^2(1-H(\phi))dx \\ & \underbrace{- \int_\Omega \left|\left\langle \nabla E, \frac{\nabla\phi}{|\nabla\phi|}\right\rangle\right| |\nabla H(\phi)|dx}_{\text{Robust Alignment}} + \underbrace{\int_\Omega \mathcal{G}(\nabla E, v_T)|\nabla H(\phi)|dx}_{\text{Geodesic Active Contour}}.\end{aligned} \tag{14}$$

When $v \approx 0$ (across edges), the third and forth terms vanish, while the first and second terms vanish within the segments whenever $v \approx 1$.

Using the alternate minimization method, we first calculate the level set function ϕ while keeping the constants $\overrightarrow{c}$ fixed. Then we keep ϕ fixed and minimize the functional with respect to each of the four constants. The implicit level set evolution takes the form

$$\begin{aligned}\phi_t = -\frac{\delta\mathcal{F}}{\delta\phi} = -\Big\{ & \lambda_1(1-v)^2(E-c_1)^2 - \lambda_2(1-v)^2(E-c_2)^2 \\ & + \lambda_3 v^2(E-c_3)^2 - \lambda_4 v^2(E-c_4) \\ & - \operatorname{sign}\left(\langle\nabla E, \nabla\phi\rangle\right)\nabla^2 E - \nabla\cdot\left(\mathcal{G}(\nabla E, v_T)\frac{\nabla\phi}{|\nabla\phi|}\right)\Big\}\,\delta(\phi).\end{aligned} \tag{15}$$

See Ref. [11] for more details on the derivation of the fifth and sixth terms. Keeping ϕ fixed and minimizing $\mathcal{F}(\phi, \overrightarrow{c})$ with respect to c_1 yields

$$c_1 = \frac{\int (1-v)^2 E H(\phi)}{\int (1-v)^2 H(\phi)}. \tag{16}$$

The constants c_2, c_3 and c_4 are calculated in the same manner. Following Chan and Vese [6], the Heaviside function H is approximated by the $C^\infty(\overline{\Omega})$ function

$$H_\varepsilon(z) = \frac{1}{2}\left(1 + \frac{2}{\pi}\arctan\left(\frac{z}{\varepsilon}\right)\right),$$

hence

$$\delta_\varepsilon(z) = \frac{d}{dz}H_\varepsilon(z) = \frac{1}{\pi}\frac{\varepsilon}{\varepsilon^2 + z^2}.$$

In our implementation we use this approximation with $\varepsilon = 1$.

Fig. 5 shows experimental results with a real image degraded by space variant defocus blur. The top-left 250×333 image was obtained with deliberate defocus blur using a Canon Power Shot G5 digital camera. The foreground object was located $1.2\,m$ in front of the background poster. The picture was taken such that only the background was in focus. The top-right image shows the recovered image using the Mumford-Shah based non-blind *space-invariant* method [2] such

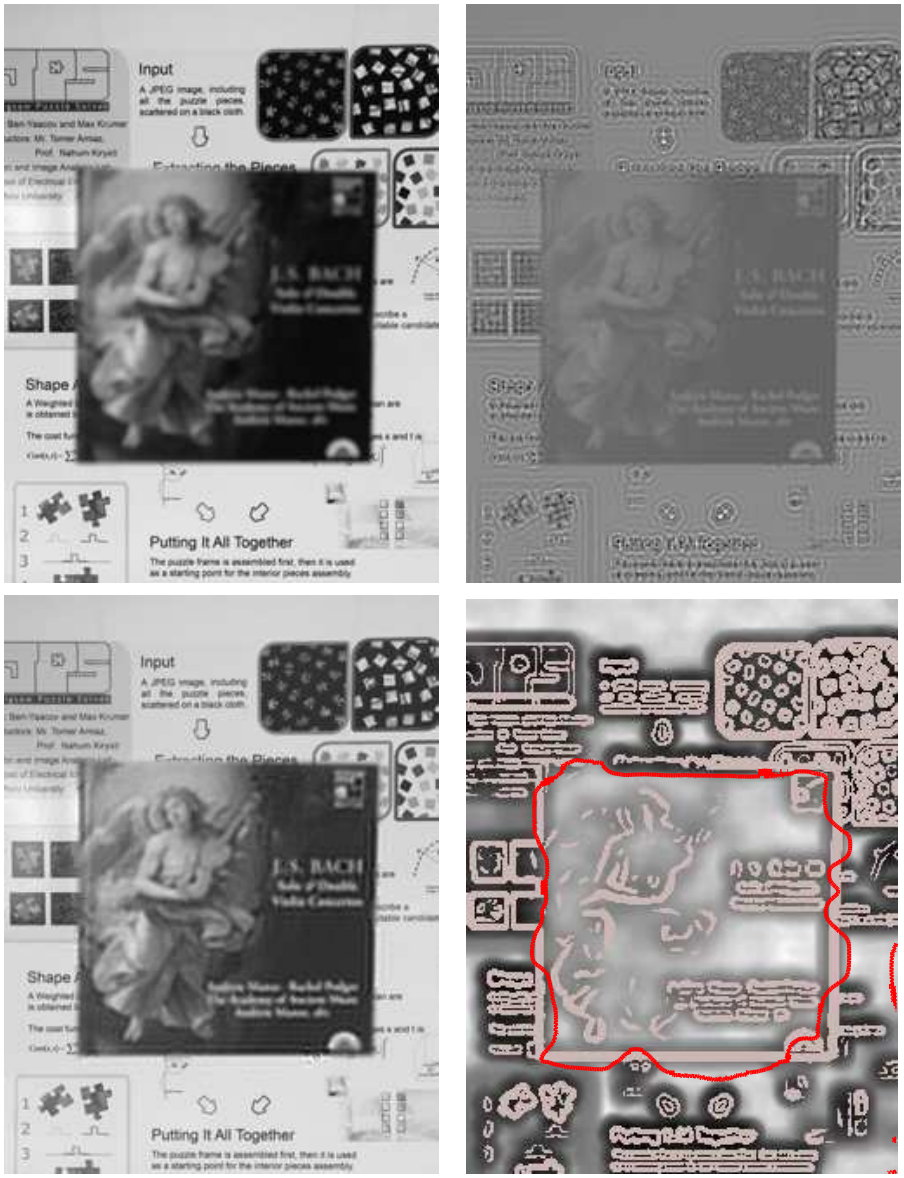

Fig. 5. Real space-variant restoration. *Top-left:* Observed image, background is in focus while foreground is out of focus. *Top-right:* Space-invariant image restoration using a single out of focus blur kernel. *Bottom-left:* Recovered image using the suggested method. *Bottom-right:* Separating contour (red) on the background of the E function and image edges (pink).

that the whole image was restored by the foreground kernel. The failure of this recovery is evident.

Better results were obtained using our space-variant method. At the first stage, the separating contour was calculated by the minimization of Eq. (14). The E function together with the binary edge map v_T and final contour, are shown bottom-right. In this case the parameter set was $\lambda_1 = \lambda_2 = 3$, $\lambda_3 = \lambda_4 = 0.1$, $\nu = 0.95$, $\mu = 14$, $\gamma = 0.6$, $T = 0.93$ and $\Delta t = 0.1$ as the gradient descent time step. The ball radius was set to 8 pixels. The background PSF was assumed to be a delta function and the foreground PSF was manually tuned to be a pill-box of radius 4. In the second stage of the restoration process, the non-blind space-variant method was employed using the calculated ϕ function with $\beta = 0.001$, $\alpha = 0.1$, $\epsilon = 0.1$, $\eta_1 = 1$, and $\eta_b = 30$. In the bottom-left is the reconstruction using the method suggested in this paper. The quality of the image obtained using the proposed method shows its applicability to real-world life situations.

4 Discussion

We presented a novel approach to space-variant deblurring of a *single* image, where region-wise space-variant point spread function is the underlying model of this research. In the non-blind space-variant restoration case, we proposed an efficient algorithm that globally recovers the image with no limitations on the number and shapes of the sub-regions. Special handling of the region boundaries is not necessary. Later, we introduced a segmentation method to determine the blur regions. The separating contour between two blurred sub-regions was represented as an evolving level set function and the blur kernels are assumed to be known or easily estimated. Promising experimental results of real and synthetic images demonstrate the potential of the suggested method to recover space-variant blurred images.

This study suggests additional challenging topics for future research. In the segmentation process, the number of blurred regions can be greater than two. The detection of the blur kernels, analysis of the algorithm in the presence of noise, convergence issues and parameters estimation can be also considered. The fully blind restoration problem is highly ill-posed, therefore sophisticated regularizers will have to be employed.

Acknowledgment

This research was supported by the A.M.N. Foundation and by MUSCLE: Multimedia Understanding through Semantics, Computation and Learning, a European Network of Excellence funded by the EC 6th Framework IST Programme.

References

1. L. Ambrosio and V.M. Tortorelli. Approximation of functionals depending on jumps by elliptic functionals via Γ-convergence. *Comm. Pure Appl. Math.*, 43(8):999–1036, 1990.

2. L. Bar, N. Sochen, and N. Kiryati. Semi-blind image restoration via Mumford-Shah regularization. *IEEE Trans. Image Processing*, 15(2):483–493, 2006.
3. A. Braides. *Approximation of Free-Discontinuity Problems*, volume 1694 of *Lecture Notes in Mathematics*, pages 47–51. Springer, 1998.
4. P. Favaro M. Burger and S. Soatto. Scene and motion reconstruction from defocused and motion-blurred images via anisotropic diffusion. In *Proc. of 8th European Conference on Computer Vision*, pages 257–269, 2004.
5. V. Caselles, R. Kimmel, and G. Sapiro. Geodesic active contours. *International Journal of Computer Vision*, 22:61–79, 1997.
6. T. Chan and L. Vese. Active contours without edges. *IEEE Trans. Image Processing*, 10:266–277, 2001.
7. P. Favaro and S. Soatto. A variational approach to scene reconstruction and image segmentation from motion-blur cues. In *Proc. of IEEE Conference on Computer Vision and Pattern Recognition*, pages 631–637, 2004.
8. P. Favaro and S. Soatto. A geometric approach to shape from defocus. *IEEE Trans. Pattern Analysis and Machine Intelligence*, 27:406–417, 2005.
9. H. Jin and P. Favaro. A variational approach to shape from defocus. In *Proc. of 7th European Conference on Computer Vision*, pages 18–30, 2002.
10. J. Kim, A. Tsai, M. Cetin, and A.S. Willsky. A curve evolution-based variational approach to simultaneous image restoration and segmentation. In *Proc. of IEEE International Conference on Image Processing*, volume 1, pages 109–112, 2002.
11. R. Kimmel. Fase edge integration. In S. Osher and N. Paragios, editors, *Geometric Level Set Methods in Imaging Vision and Graphics*. Springer-Verlag, 2003.
12. T. Lauer. Deconvolution with a spatially-variant PSF. In *Proc. of the SPIE, Astronomical Data Analysis II.*, pages 167–173, 2002.
13. D. Mumford and J. Shah. Optimal approximations by piecewise smooth functions and associated variational problems. *Comm. Pure Appl. Math.*, 42:577–685, 1989.
14. J.G. Nagy and D.P. Oĺeary. Restoring images degraded by spatially-variant blur. *Siam Journal on Scientific Computing*, 19:1063–1082, 1998.
15. S. Osher and J.A. Sethian. Fronts propagating with curvature-dependent speed: Algorithms based on hamilton-jacobi formulation. *Journal of Computational Physics*, 79:12–49, 1988.
16. P. Perona and J. Malik. Scale-space and edge detection using anisotropic diffusion. *IEEE Trans. Pattern Analysis and Machine Intelligence*, 12:629–639, 1990.
17. L.I. Rudin, S. Osher, and E. Fatemi. Non linear total variatrion based noise removal algorithms. *Physica D*, 60:259–268, 1992.
18. Y. Schechner, N. Kiryati, and R. Basri. Separation of transparent layers using focus. *International Journal of Computer Vision*, 39:25–39, 2000.
19. C.R. Vogel and M.E. Oman. Fast, robust total variation-based reconstruction of noisy, blurred images. *IEEE Trans. Image Processing*, 7:813–824, 1998.
20. M. Welk, D. Theis, and J. Weickert. Variational deblurring of images with uncertain and spatially variant blurs. In *Pattern Recognition, 27th DAGM Symposium*, volume 3663 of *LNCS*, pages 485–492, 2005.
21. W. Xia, R. M. Lewitt, and P. R. Edholm. Fourier correction for spatially variant collimator blurring in SPECT. *IEEE Trans. Medical Imaging*, 14:100–115, 1995.
22. Y. You and M. Kaveh. Blind image restoration by anistropic regularization. *IEEE Trans. Image Processing*, 8:396–407, 1999.